10.1098/rsta.2003.1216

THE ROYAL SOCIETY

Managing photons for quantum information processing

By Alfred B. U'Ren, Eran Mukamel, Konrad Banaszek and Ian A. Walmsley

Clarendon Laboratory, University of Oxford, Oxford OX1 3PU, UK

Published online 2 June 2003

We study distinguishing information in the context of photonic quantum interference tailored for practical implementations of quantum information processing schemes. In particular, we consider the character of single-photon states optimized for multiple-source interference experiments and for experiments relying on Bell-state measurement and arrive at specific design criteria for photons produced by parametric down-conversion. Such states can be realistically implemented with available technology. We describe a novel method for characterizing the mode structure of single photons, and demonstrate it in the context of coherent light.

Keywords: parametric down-conversion; quantum communication; Bell-state measurement

1. Introduction

Among physical systems that can be used for practical realizations of novel information processing schemes based on intrinsically quantum phenomena, photons are the primary candidates for constituting carriers of quantum information. Applications of photons as 'flying qubits' include quantum cryptography, communication between distributed computational nodes in quantum networks, as well as elementary building blocks for registers in all-optical quantum computation.

Using single photons as carriers of qubits in quantum information processing requires, in most cases, that they be made to interact in a controlled coherent way. This is usually facilitated by modal interference which is, however, critically sensitive to the spatio-temporal structure of the interfering photons. Great care must therefore be exercised in making sure that no distinguishing information is contained in the interfering photons that would allow one to trace their origin. A common approach to cope with this problem is the implementation of strong spatial and spectral filtering. Such a method, however, reduces the available photon sample, and also contributes deleteriously to the overall detection efficiency. Overcoming the limitations of this approach is currently one of the main challenges in the further development of quantum information processing applications in the photonic domain.

The generation of entanglement relies on the coherent addition of two or more quantum amplitudes resulting from interfering pathways. This interference

One contribution of 20 to a Discussion Meeting 'Practical realizations of quantum information processing'.

is degraded and indeed can be destroyed by distinguishing information even if no explicit use is made of this information. It is therefore crucial to develop the ability to manage distinguishing information in all photonic degrees of freedom. The purpose of this paper is to explore methods for engineering the modal structure of photon sources. The physical process that we will consider is spontaneous parametric down-conversion (PDC), which has been the primary source of non-classical optical radiation in recent quantum information experiments. Our goal is to develop photon sources that produce photons in well-specified single spatio-temporal modes such that the resulting engineered photons have identical mode structures, with, in principle, no distinguishing information residing in any degree of freedom, thus ensuring high visibility interference.

2. Criteria for the design of photon states

(a) *Design criteria for photon states to be used in multiple-crystal interferometry*

A basic requirement necessary for the successful implementation of photon-based quantum computation is the availability of multiple-photon entangled states. In this section we explore the experimental challenges likely to be faced when synthesizing such a multiple-photon state employing a number of two-photon sources pumped synchronously with an ultrashort pulsed pump. Through such an approach, distinguishing information implicit in timing can be limited to the pulsed-pump temporal duration. Though it is rather difficult to view such an approach based on PDC as a practical route towards fully scalable all-optical quantum computation, it can be reasonably expected that this process can be applied in small-scale quantum circuits used for example in quantum communications.

A two-photon PDC state can in general be expressed as a weighted sum of creation operators acting on a vacuum,

$$|\Psi\rangle = \sum_{\mu_\mathrm{s}} \sum_{\mu_\mathrm{i}} \int_0^\infty \mathrm{d}\omega_\mathrm{s} \int_0^\infty \mathrm{d}\omega_\mathrm{i} \times \int \mathrm{d}\boldsymbol{k}_\mathrm{s}^\perp \int \mathrm{d}\boldsymbol{k}_\mathrm{i}^\perp \, S(\omega_\mathrm{s}, \boldsymbol{k}_\mathrm{s}^\perp, \mu_\mathrm{s}; \omega_\mathrm{i}, \boldsymbol{k}_\mathrm{i}^\perp, \mu_\mathrm{i}) \hat{a}^\dagger_{\boldsymbol{k}_\mathrm{s}^\perp \mu_\mathrm{s}}(\omega_\mathrm{s}) \hat{a}^\dagger_{\boldsymbol{k}_\mathrm{i}^\perp \mu_\mathrm{i}}(\omega_\mathrm{i}) |\mathrm{vac}\rangle, \quad (2.1)$$

where the function $S(\omega_\mathrm{s}, \boldsymbol{k}_\mathrm{s}^\perp, \mu_\mathrm{s}; \omega_\mathrm{i}, \boldsymbol{k}_\mathrm{i}^\perp, \mu_\mathrm{i})$ represents the joint two-photon amplitude in terms of the photon degrees of freedom: frequency, transverse momentum (with respect to the pump field) and polarization. The two-photon probability amplitude depends on the form of the pump field and on the so-called phase-matching function, defined by the optical properties of the crystal. Throughout the remaining discussion, it is assumed that the signal and idler directions of propagation are fixed, e.g. with pinholes.

What are the requirements on the spectral state for a photon pair to exhibit high-visibility interference? The answer depends on which experiment we wish to perform. For the classical Hong–Ou–Mandel interferometer (HOMI) (Hong *et al.* 1987), it turns out that the fourth-order interference visibility depends only on the degree to which the joint spectral amplitude is symmetric (here symmetry is defined for our purposes as $S(\omega_\mathrm{s}, \omega_\mathrm{i}) = S(\omega_\mathrm{i}, \omega_\mathrm{s})$).

As an example of a multi-crystal experiment, let us now discuss a two-PDC crystal apparatus in an event-ready HOMI-like arrangement, as shown in figure 1*a*. The

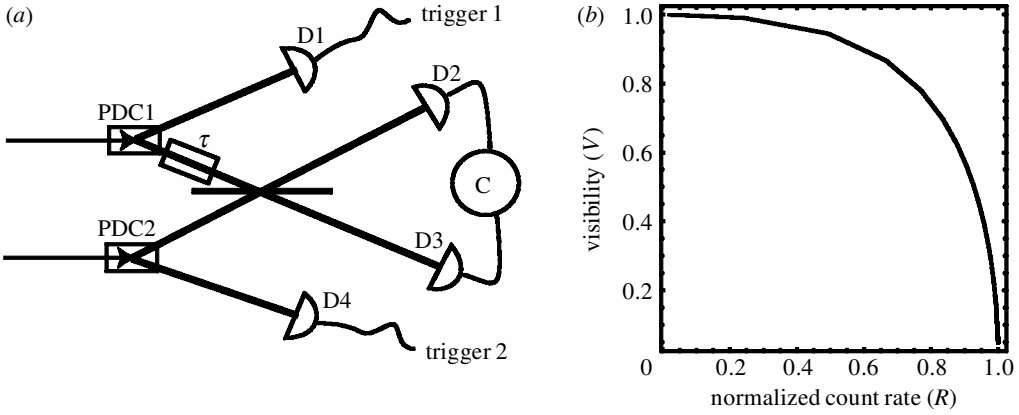

Figure 1. (*a*) Two-PDC crystal HOMI arrangement. Interference visibility is reduced if the photon pairs are spectrally correlated. (*b*) Trade-off between interference visibility and count rate.

idler photon from the first crystal is interfered with the signal photon from the second crystal, while the remaining two channels are used as triggers. The experiment consists of monitoring quadruple coincidences on D1 through D4, while scanning the delay τ. If both PDC crystals are identical and described by a joint spectral amplitude function $f(\omega_\mathrm{s}, \omega_\mathrm{i})$, the four-fold coincidence rate $R_\mathrm{c}(\tau)$ may be shown to be (Grice 1997)

$$R_\mathrm{c}(\tau) \propto \int_0^\infty \int_0^\infty \int_0^\infty \int_0^\infty \mathrm{d}\omega_1\, \mathrm{d}\omega_2\, \mathrm{d}\omega_3\, \mathrm{d}\omega_4\, f(\omega_1, \omega_2) f(\omega_3, \omega_4) \times [f^*(\omega_1, \omega_2) f^*(\omega_3, \omega_4) - \mathrm{e}^{\mathrm{i}(\omega_1 - \omega_3)\tau} f^*(\omega_1, \omega_4) f^*(\omega_3, \omega_2)]. \quad (2.2)$$

The visibility becomes unity if at $\tau = 0$ the coincidence rate vanishes; we can see from equation (2.2) that a sufficient condition for this to occur is given by

$$f(\omega_1, \omega_2) f(\omega_3, \omega_4) = f(\omega_1, \omega_4) f(\omega_3, \omega_2). \quad (2.3)$$

Unlike in the (one-crystal) HOMI, symmetry in the function $f(\omega_\mathrm{s}, \omega_\mathrm{i})$ does not help in fulfilling this condition. It may be seen, however, that such a condition is met if functions $p(\omega)$ and $q(\omega)$ exist such that $f(\omega_\mathrm{s}, \omega_\mathrm{i}) = p(\omega_\mathrm{s}) q(\omega_\mathrm{i})$. The latter is true if the photon pair is spectrally uncorrelated.

How can we obtain such a factorizable state? Perhaps the simplest way is by making use of spectral and/or spatial filtering. A recent experiment by Lvovsky *et al.* (2001) demonstrates the way in which distinguishing information can be thus eliminated, but at the cost of extremely low resultant production rates. Consider a simplified type-I source where the joint spectral amplitude is approximated by a Gaussian (i.e. we neglect the secondary peaks of the sinc function and neglect dispersive effects) and is spectrally filtered,

$$f(\nu_\mathrm{s}, \nu_\mathrm{i}) = A \exp\left[-2(\nu_\mathrm{s}^2 + \nu_\mathrm{i}^2)\left(\frac{1}{\sigma_\mathrm{F}^2} + \frac{1}{\sigma^2}\right) - \frac{2\nu_\mathrm{s}\nu_\mathrm{i}}{\sigma^2}\right], \quad (2.4)$$

where A is a normalization constant, $\nu_j = \omega_j - \omega_0$, σ_F is the width of the Gaussian spectral filter and σ is the resultant width of the product of the pump-envelope

and phase-matching functions. Substituting equation (2.4) into equation (2.2) and integrating yields

$$R_{\mathrm{c}}(\tau) \propto R_0\left[1 - V\exp\left(-\frac{\sigma^2\sigma_{\mathrm{F}}^2\tau^2}{8(\sigma_{\mathrm{F}}^2+\sigma^2)}\right)\right], \tag{2.5}$$

which represents an interference dip with visibility

$$V = \sqrt{1 - \frac{\sigma_{\mathrm{F}}^4}{(\sigma_{\mathrm{F}}^2+\sigma^2)^2}}, \tag{2.6}$$

and a normalized count rate

$$R_0 = \frac{2\sigma_{\mathrm{F}}^2}{2\sigma_{\mathrm{F}}^2+\sigma^2}, \tag{2.7}$$

which has a value between 0 and 1. For a fixed value of σ, the filtering strength determines the value of R_0, which vanishes for strong filtering ($\sigma_{\mathrm{F}} \ll \sigma$) and gives unity in the limit of no filtering ($\sigma_{\mathrm{F}} \gg \sigma$).

As expected, in the strong-filtering regime (i.e. $\sigma_{\mathrm{F}} \ll \sigma$), equation (2.6) predicts unit visibility. Filtering, however, has the unfortunate consequence that the count rate is prohibitively reduced by rejecting most photon pairs. This is illustrated in figure 1*b*, which shows the relationship between the visibility (see equation (2.6)) in the two-crystal HOMI and the expected count rate (see equation (2.7)) with each point along the curve corresponding to a different filtering strength.

(*b*) *Design criteria for polarization-entangled states*

The polarization of light fields can be readily controlled using, for example, wave plates and polarizers. This is in marked contrast with the case of other photonic degrees of freedom, such as frequency, for which it is rather more difficult to achieve a comparable level of control. It is therefore not surprising that most recent experiments exploring issues of entanglement have relied on polarization entanglement. A number of reliable methods for generating polarization-entangled photon pairs have been proposed and implemented (e.g. Kwiat *et al*. 1995, 1999).

As in any interference experiment, a pre-condition for high interference visibility is that distinguishing information between the interfering pathways is eliminated, even in those degrees of freedom which are not of primary interest for the experiment in question. This applies to the generation of polarization-entangled photon pairs, where, even though polarization is the degree of freedom of interest, it is crucial to engineer the spectral properties of the photon pairs appropriately to eliminate any spectral distinguishing information.

We will illustrate the importance of this point by studying the Braunstein–Mann Bell-state analyser (Braunstein & Mann 1995). The apparatus is displayed in figure 2*a*, where 'BS' is a 50:50 beam-splitter and 'PBS1' and 'PBS2' are polarizing beam-splitters. This experiment serves as a building block for a large class of experiments relying on Bell-state measurement, such as entanglement swapping and teleportation. Employing such an analyser, the experimenter can make inferences about the state of the incoming photon pair from the firing pattern of the four detectors. Likewise, knowing the state of the incoming photon pair, inferences can be made about what the firing pattern will be. For instance, assuming that there is zero delay

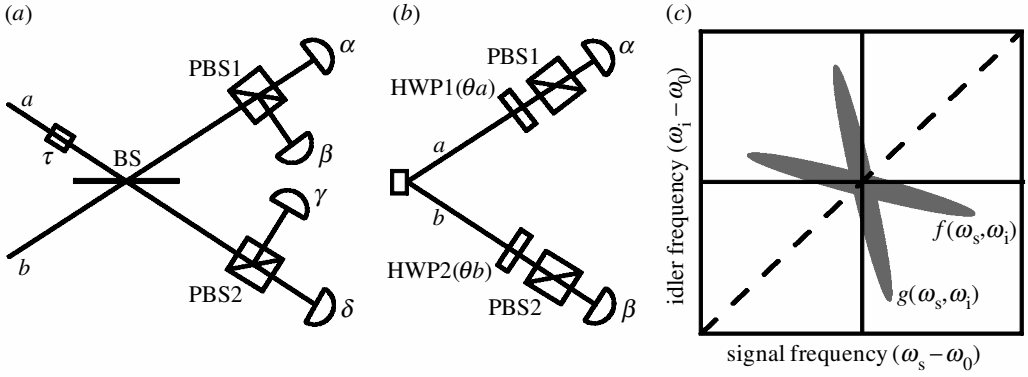

Figure 2. (*a*) Braunstein–Mann Bell-state analyser; (*b*) polarization-correlation experiment; and (*c*) graphical representation of the condition for optimal performance.

between the two photons ($\tau = 0$), if α and γ or β and δ fire we then know with certainty that the incoming state is the singlet state $|\psi^{(-)}\rangle_{ab} = 2^{-1/2}(|HV\rangle_{ab} - |VH\rangle_{ab})$. Likewise, if the incoming state is $|\psi^{(+)}\rangle_{ab} = 2^{-1/2}(|HV\rangle_{ab} + |VH\rangle_{ab})$, we can infer with certainty that either α and β or δ and γ will fire. Considering the fact that the Bell-state analyser relies on quantum interference, we would expect that, if the two-photon state used were to exhibit spectral distinguishing information, the correlation between the incoming two-photon state and the firing pattern would no longer be perfect. We will compare the behaviour of the Bell-state analyser with that of the apparatus shown in figure 2*b*, which measures the polarization correlations present in a polarization-entangled two-photon state.

We begin our analysis by considering a maximally entangled polarization Bell state with the spectral component of the state included in the explicit form

$$|\psi^{\pm}\rangle = \frac{1}{\sqrt{2}} \int_0^\infty \int_0^\infty \mathrm{d}\omega_1 \, \mathrm{d}\omega_2 [f(\omega_1, \omega_2) a_{\mathrm{H}}^\dagger(\omega_1) b_{\mathrm{V}}^\dagger(\omega_2) \pm g(\omega_1, \omega_2) a_{\mathrm{V}}^\dagger(\omega_1) b_{\mathrm{H}}^\dagger(\omega_2)] |\mathrm{vac}\rangle, \tag{2.8}$$

where a and b refer to two distinct spatial modes, where 'H' and 'V' refer to horizontal and vertical polarization and where the functions $f(\omega_1, \omega_2)$ and $g(\omega_1, \omega_2)$ are each normalized such that the integral over both arguments of the modulus squared of the function is unity. In order to study the performance of the Bell-state analyser, we detect the whole output from each port of the beam-splitter in figure 2*a*, i.e. we remove the two polarizing beam-splitters and place a detector in each output mode. If the Bell-state analyser operates ideally, as described above, the singlet $|\psi^{(-)}\rangle$ state yields a unit coincidence rate, while the $|\psi^{(+)}\rangle$ yields a zero coincidence rate. On the other hand, by calculating the coincidence rate assuming a (non-ideal) incoming state given as in equation (2.8), we obtain the result

$$R_{\mathrm{c}}^{\pm}(\tau) = \frac{1}{4} \int_0^\infty \int_0^\infty \mathrm{d}\omega_1 \, \mathrm{d}\omega_2 \, |f(\omega_1, \omega_2) \mp \mathrm{e}^{\mathrm{i}(\omega_1 - \omega_2)\tau} g(\omega_2, \omega_1)|^2, \tag{2.9}$$

where the '$\pm$' on the left-hand side refers to a $\psi^{(+)}/\psi^{(-)}$ incoming state. Because the integrand in equation (2.9) is non-negative, the necessary and sufficient condition to obtain $R_{\mathrm{c}}^{+} = 0$ and $R_{\mathrm{c}}^{-} = 1$ at $\tau = 0$ (i.e. the desired behaviour) is given by

$$g(\omega_1, \omega_2) = f(\omega_2, \omega_1). \tag{2.10}$$

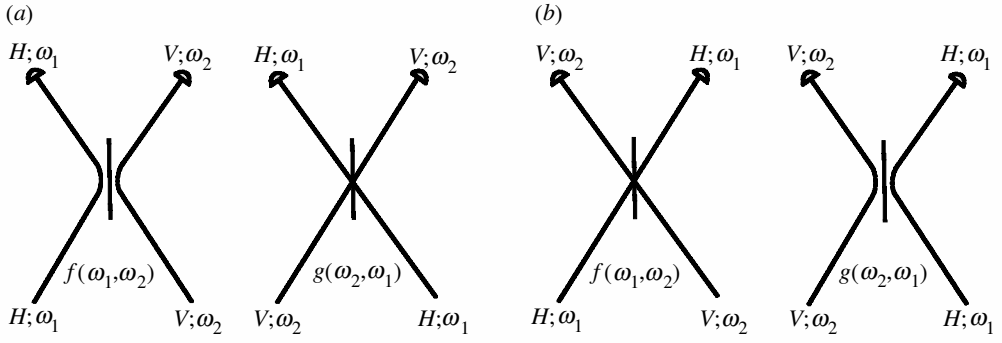

Figure 3. The two Feynman alternatives shown in (*a*) and (*b*) are indistinguishable from each other.

Figure 2*c* depicts the condition in equation (2.10) graphically: the two spectral amplitude functions must be the specular image of each other across the line $\omega_1 = \omega_2$. In order to gain a physical understanding of this condition we consider the Feynman alternatives leading to obtaining a coincidence event. Suppose that the photon pair is described by the first component of the Bell state, i.e. the amplitude containing $f(\omega_1, \omega_2)$ and that the two photons are reflected at the beam splitter. Such an event (left-hand diagram in figure 3*a*) is indistinguishable (meaning it has an identical detection pattern) from the event where the photon pair is described by the second amplitude with reversed frequency arguments, i.e. $g(\omega_2, \omega_1)$, and where the two photons are transmitted at the beam splitter (right-hand diagram in figure 3*a*). For this system, there is a second set of two pathways, as shown in figure 3*b*, which may lead to a coincidence. For unit interference visibility to occur, the two pathways in each set must be indistinguishable from each other. Figure 3 shows schematically that, for both sets of pathways, indistinguishability is guaranteed (for $\tau = 0$) if the condition in equation (2.10) is fulfilled.

Consider now the apparatus in figure 2*b*, which has been used in several recent experiments to test whether a photon pair is polarization entangled. Assuming that the incoming state is given as in equation (2.8), the coincidence rate as a function of the polarization rotation angles in each arm, θ_a and θ_b, may be shown to be

$$R_{\mathrm{c}}^{\pm}(\theta_a, \theta_b) = \int_0^\infty \int_0^\infty \mathrm{d}\omega_1 \, \mathrm{d}\omega_2 \, | \cos\theta_a \sin\theta_b f(\omega_1, \omega_2) \pm \sin\theta_a \cos\theta_b \, g(\omega_1, \omega_2)|^2. \tag{2.11}$$

The resulting necessary and sufficient condition to obtain unit visibility fringes (in which case the coincidence rate reduces to $R_{\mathrm{c}}^{\pm} = \sin^2(\theta_a \pm \theta_b)$) is

$$f(\omega_1, \omega_2) = g(\omega_1, \omega_2). \tag{2.12}$$

Note that this condition, which says that the two amplitudes should be identical, is different from that derived for the Bell-state analyser experiment (see equation (2.10)). The fact that these conditions differ means that, depending on the kind of experiment to be performed, the polarization-entangled state to be used should entail differently engineered spectral properties.

Is it possible to fulfil both conditions simultaneously? Together, the two conditions reduce to the requirement that the quantum amplitude be symmetric,

i.e. $f(\omega_1, \omega_2) = f(\omega_2, \omega_1)$. By generating a polarization-entangled state using two type-I cascaded crystals (Kwiat *et al.* 1999), the two amplitudes $f(\omega_1, \omega_2)$ and $g(\omega_1, \omega_2)$ are each symmetric and can be made to be identical, even in the case where a pulsed pump is used, if the pump is pre-compensated, as described by Nambu *et al.* (2002). Therefore, this method for generating polarization-entangled states has the important property that it can be made to fulfil both conditions, so that the same source may be used successfully (without the need for spectral filtering) for the polarization-correlation experiment (figure 2*a*) and for the Bell-state-analyser experiment (figure 2*b*).

Polarization-entangled photon pairs may also be synthesized using the modes defined by the intersections of the 'e'-ray and 'o'-ray cones in type-II PDC (Kwiat *et al.* 1995). It may be shown that this scheme produces a polarization-entangled state such that the condition in equation (2.10) is fulfilled. This means that such a state is well-suited for Bell-state-measurement experiments (e.g. the Bell-state analyser in figure 2*a*), while it is not well suited for the polarization-correlation experiment (figure 2*b*). In a recent experiment making use of this type-II source (Kim *et al.* 2003; Kim & Grice 2002), one of the two spatial modes is subjected to a 90° polarization rotation prior to be being combined at a beam-splitter with the other mode. The authors show that the two output modes from the beam-splitter are in a polarization-entangled state which yields near-unit visibility, without resorting to spectral filtering, in a polarization-correlation experiment such as the one shown in figure 2*b*. We can understand the results of Kim *et al.* (2003) in terms of the conditions in equations (2.10) and (2.12). The half-wave plate and beam-splitter accomplish turning a state obeying $f(\omega_1, \omega_2) = g(\omega_2, \omega_1)$ into a state obeying $f(\omega_1, \omega_2) = g(\omega_1, \omega_2)$. The resulting state, however, is no longer well suited for Bell-measurement experiments.

It would therefore appear that it is possible to optimize a polarization-entangled photon pair generated via type-II PDC for one of the two types of experiments discussed above, but not for both simultaneously. There are in fact two ways in which the amplitudes may be made identical and symmetric, and therefore be made to fulfil both conditions. The first is by pumping the type-II source with a continuous-wave (CW) pump: in the limit of zero pump bandwidth, the pump-envelope function, which is always symmetric, dominates over the phase-matching function to determine the overall spectral amplitude. It is also possible to symmetrize the amplitudes by placing a (symmetric) interference filter with a narrow-enough bandwidth and an appropriately chosen central bandpass frequency at each of the two spatial modes—the latter, of course, at the cost of a sharp reduction in the production rate of photon pairs. We therefore conclude that an ultrafast-pumped spectrally unfiltered type-II polarization-entangled source cannot be simultaneously optimized for both kinds of experiments, in contrast with a cascaded type-I two-crystal source.

3. Characterization of spatial coherence

In addition to the spectral degree of freedom discussed in the preceding section, the spatial structure of the photons, characterized by the distribution of their transverse momenta, plays an equally important role in multi-photon interference. In most experiments on photonic quantum information processing, photons generated in down-conversion are coupled into single-mode fibres. This enables their transmission over relatively long distances without significant losses, and also greatly sim-

plifies alignment of interferometric set-ups used for detection, such as the Bell-state analyser proposed in Braunstein & Mann (1995) and used in a number of experiments on teleportation and entanglement swapping. In order to ensure good coupling efficiency, the down-converted photons should be generated optimally in single spatial modes that could be transformed using passive optics into the fibre eigenmodes. This brings us to the issue of characterizing transverse spatial coherence of single-photon signals, which would be a useful diagnostic technique in quantum interference experiments with down-converted photons.

Determination of the spatial coherence of optical beams has been a subject of research in the past, and a number of practical schemes have been proposed (Brenner & Lohmann 1982; Iaconis & Walmsley 1996; Wax & Thomas 1996; Dorrer & Walmsley 2002). Most of them, however, are based on array detection, which is not easily implementable for single-photon signals. Of course, an array detector can in principle always be replaced with a single scanning detector, but this approach results in a loss of signal photons and therefore it lowers the signal-to-noise ratio significantly. We have recently demonstrated a novel technique for measuring spatial coherence, which uses a single area-integrating detector collecting the output light. This improves the signal-to-noise ratio, similarly to the case of Fourier transform spectroscopy, which is beneficial in regimes when array detectors are not available. A natural representation for spatial coherence that appears in this method is the Wigner distribution function (Bastiaans 1978).

The basic idea of the method is to measure interference between two replicas of the input wavefront that are displaced in the phase space and then mutually rotated by 180°. The phase-space displacement can easily be realized for the spatial degree of freedom by a simple steering of the beam, and the rotation is implemented using reflections. We note that a similar idea underlies a previous measurement of the Wigner function for the quadrature degree of freedom of a single light mode (Banaszek & Wódkiewicz 1996).

The complete set-up built to measure the Wigner distribution function is depicted in figure 4. For simplicity, we consider here only a single transverse degree of freedom in the plane of the figure; the two-dimensional generalization is straightforward. The input beam is steered using the mirror M1 into a three-mirror Sagnac interferometer. The displacement and the tilt of the mirror transform the input field according to

$$E(\xi) \rightarrow \mathrm{e}^{\mathrm{i}k\xi} E(\xi + x), \tag{3.1}$$

and thus control the point (x, k) at which the Wigner function is measured. The 50:50 beam splitter BS generates a pair of replicas of the displaced and tilted input beam travelling in the opposite directions. The interferometer contains a Dove prism whose base forms 45° with the plane of the interferometer. Transmission through the Dove prism rotates each of the counterpropagating beams by 90°, which adds up to the 180° relative rotation required to measure the Wigner function. The operation of the set-up can be most easily understood by analysing propagation of the replicas of an exemplary image through the interferometer, as shown in figure 4*b*. The counterpropagating replicas of the input field are recombined at the output port of the interferometer, and the emerging beam is focused with the help of a lens on an area-integrating detector.

The intensity recorded by the detector can be decomposed into a sum of three terms. Two of them correspond to the detection of each of the replicas separately,

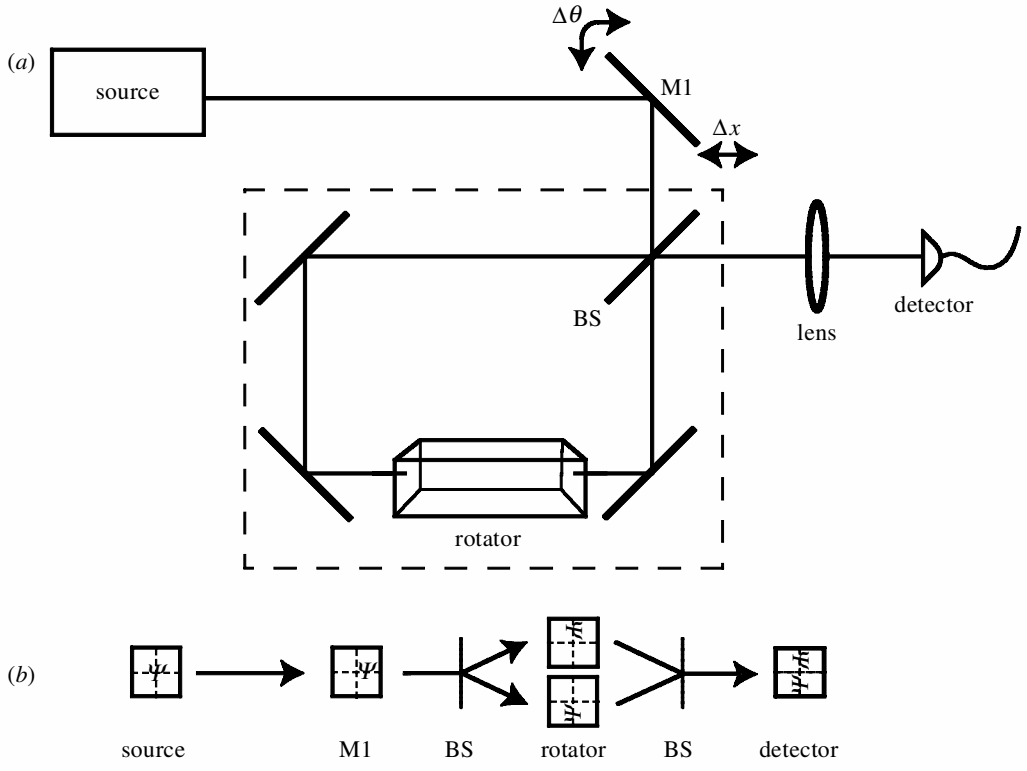

Figure 4. (*a*) Experimental set-up for measuring the spatial Wigner distribution function using an area-integrating detector. (*b*) Schematic of transformations of the wavefront propagating through the set-up.

and they remain constant as long as the aperture of the interferometer does not clip off any of the input field. The third term, I_{12}, originating from the interference between the counterpropagating replicas is proportional to

$$I_{12} \propto \int \mathrm{d}\xi \, [\mathrm{e}^{-\mathrm{i}k\xi} E(-\xi + x)]^* \, \mathrm{e}^{\mathrm{i}k\xi} E(\xi + x), \tag{3.2}$$

and it is straightforward to verify that the right-hand side expression is the definition of the Wigner function for the point (x, k). The complete Wigner function can be therefore scanned by measuring the detector photocurrent as a function of the position and the tilt of the steering mirror, and subtracting the constant pedestal. In figure 5 we depict exemplary results, obtained for a He–Ne laser beam filtered through a single-mode fibre and reflected from the front and the back surfaces of a tilted glass wedge. The measured Wigner distribution function shows two slightly converging Gaussian beams with different transverse wave vectors, where the oscillating pattern located between the Gaussians is a signature of their mutual coherence. An additional feature is the presence of faint ripples on one of the Gaussian peaks, at twice the spatial frequency of the fringe pattern at the centre of the distribution. These ripples can be attributed to interference with a third, much weaker, beam generated by a secondary reflection from the glass wedge. Obviously, the same set-up can be used to characterize transverse spatial coherence of single-photon wave

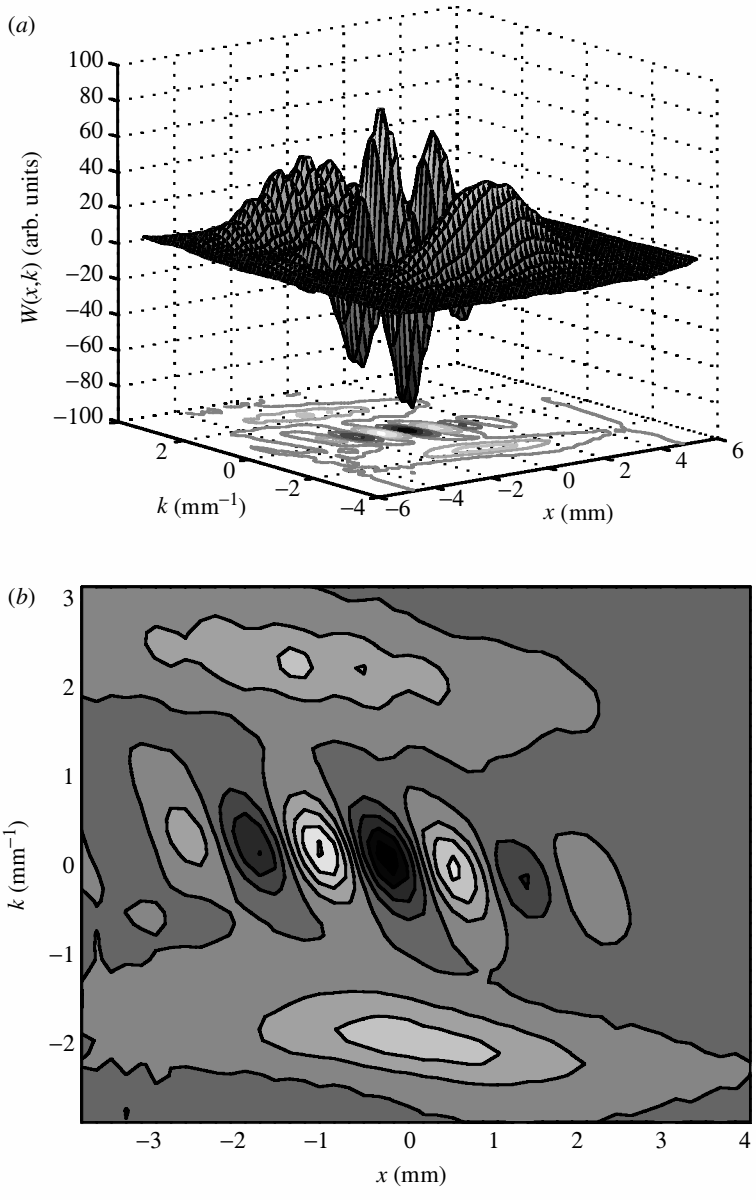

Figure 5. (*a*) Surface and (*b*) contour plots of an experimentally determined Wigner function for a beam obtained by a double reflection from a glass wedge.

packets if the output detector is replaced with an avalanche photodiode operated in the Geiger mode.

4. Engineering sources without spectral correlations

Our approach is to investigate ways to engineer the state *at the source* in order to obtain a factorizable state, thus eliminating the need for filtering. One such approach is described in Grice *et al.* (2001), where it is shown that, for degenerate collinear

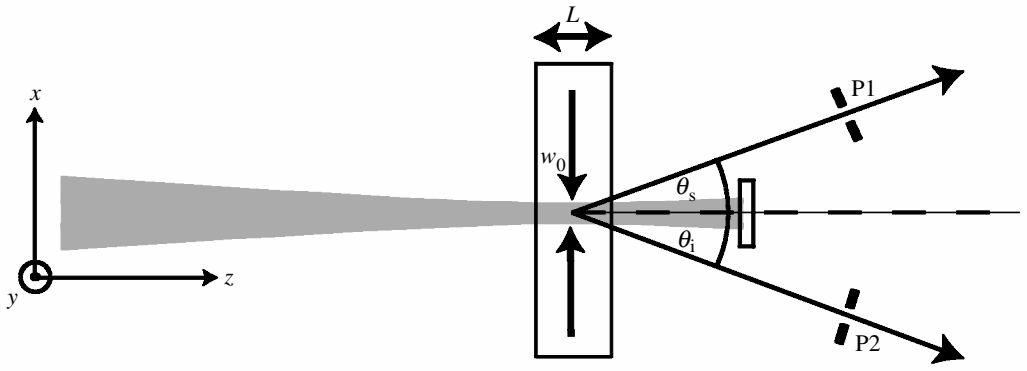

Figure 6. Uncorrelated photon-pair generation.

type-II phase matching, and for an appropriate choice of material, central PDC wavelength, crystal length and pump bandwidth, it is indeed possible to obtain such a spectrally uncorrelated state. Unfortunately, this approach works at longer wavelengths (greater than 1 μm), where single-photon detectors are not technologically well developed.

Here we present a novel method for generating spectrally uncorrelated pairs making use of non-collinear, degenerate type-I PDC in bulk crystals and which exploits the transverse momentum of the photons. This approach requires the ability to specify the crystal length and the beam diameter at the beam waist (i.e. the focusing strength) accurately and requires the spatial modes exiting the crystal to be accurately defined, for example with pinholes or fibres. An additional requirement is an ultrafast pulsed pump. Figure 6 outlines the experimental set-up. This method can be made to work at any PDC central wavelength where phase matching is possible, in particular at those wavelengths where silicon-based single-photon counting modules work efficiently.

We begin by extending the phase-matching function to the case where a Gaussian beam, rather than a plane wave, is used as the pump field. In this case the electric field amplitude is given by

$$\alpha(x,y,z;k) = \frac{1}{1+(\mathrm{i}z)/(kw_0^2)} \exp\left(-\frac{x^2+y^2}{w_0^2(1+2\mathrm{i}z/(kw_0^2))}\right) \mathrm{e}^{\mathrm{i}kz}, \tag{4.1}$$

where w_0 is the beam diameter at the beam waist. Following the procedure sketched out in Grice & Walmsley (1997), for the phase-matching function we obtain

$$\phi(\Delta k_z, \Delta k^{\perp}) \propto \exp\left(-\frac{(\Delta k^{\perp})^2 w_0^2}{4}\right) \mathrm{sinc}\left[\left(\frac{(\Delta k^{\perp})^2}{4k} - \frac{\Delta k_z}{2}\right)L\right], \tag{4.2}$$

where $\Delta k^{\perp}$ refers to the transverse momentum along the (x,z)-plane (see figure 6), so it is a scalar quantity. By making the approximation $\mathrm{sinc}(x) \approx \exp(-\gamma x^2)$ (with $\gamma = 0.193\ldots$) and the further approximation $w_0/L \gg \sqrt{\gamma}\sin^2\theta$, where θ is the propagation angle (which sets an upper limit on the focusing strength), the transverse momentum and longitudinal momentum contributions can be factorized as

$\phi(\Delta k_z, \Delta k_\perp) \propto \phi_z(\Delta k_z)\phi^\perp(\Delta k^\perp)$, where

$$\phi_z(\Delta k_z) = \exp(-\tfrac{1}{4}\gamma \Delta k_z^2 L^2), \tag{4.3}$$

$$\phi^\perp(\Delta k^\perp) = \exp(-\tfrac{1}{4}(\Delta k^\perp)^2 w_0^2). \tag{4.4}$$

The joint spectral amplitude can now be written as

$$S(\omega_\mathrm{s}, \omega_\mathrm{i}) = \alpha(\omega_\mathrm{s} + \omega_\mathrm{i})\phi_z(\Delta k_z)\phi^\perp(\Delta k^\perp),$$

where $\alpha(\omega_\mathrm{s} + \omega_\mathrm{i})$ is the pump-envelope function.

Let us restrict our attention to the case where the photons are emitted along the (x, z)-plane (see figure 6), so that the direction of propagation of a given photon can be described with the polar angle θ (and having zero azimuthal angle $\phi = 0$). We assume that the pump propagates such that $\theta_\mathrm{p} = 0$, in which case conservation of transverse momentum dictates that $\theta_\mathrm{s} = -\theta_\mathrm{i} = \theta$. Performing a Taylor expansion and neglecting second- and higher-order terms, the longitudinal and transverse phase mismatch are then given by

$$\Delta k_z = \Delta k_z^{(0)} + (k_\mathrm{p}' - k' \cos\theta)(\nu_\mathrm{s} + \nu_\mathrm{i}), \tag{4.5}$$

$$\Delta k^\perp = -k' \sin\theta(\nu_\mathrm{s} - \nu_\mathrm{i}), \tag{4.6}$$

where $\nu_j = \omega_j - \omega_0$ with $j = \mathrm{s}, \mathrm{i}$. All wavevector amplitudes and their derivatives are evaluated at ω_0 (or $2\omega_0$ in the case of k_p and k_p'). $\Delta k_z^{(0)} = k_\mathrm{p} - 2k\cos\theta$ represents a constant term which must vanish to ensure phase matching. The central idea of this approach is to exploit the fact that (as expressed in equations (4.5) and (4.6)), whereas the longitudinal phase mismatch depends on frequency sum $\nu_\mathrm{s} + \nu_\mathrm{i}$, the transverse phase mismatch depends on the frequency difference $\nu_\mathrm{s} - \nu_\mathrm{i}$. This means that, while the contours of the longitudinal phase-matching function $\phi_z(\Delta k_z)$ have negative unit slope, those of the transverse phase-matching function $\phi^\perp(\Delta k^\perp)$ have positive unit slope. Therefore, through an appropriate choice of the widths of the two functions (proportional to L^{-1} and w_0^{-1}, respectively), the overall phase-matching function can be made factorizable. The physical reason behind the positive slope of the transverse phase-matching function is that transverse momentum conservation leads to the signal and idler photons propagating on opposite sides of the pump, i.e. $\theta_\mathrm{s} = -\theta_\mathrm{i}$.

When substituting equation (4.5) into equation (4.3) and equation (4.6) into equation (4.4), and multiplying the two resulting functions, there is a cross-term proportional to $\nu_\mathrm{s}\nu_\mathrm{i}$ in the exponential argument which is responsible for the non-factorizability of the phase-matching function. Our approach is to let this term vanish, thus imposing a constraint on the crystal length L and the beam diameter at the beam waist, w_0. This constraint tells the experimenter, for a given crystal length, the required focusing strength

$$\frac{w_0}{L} = \frac{\sqrt{\gamma}(k_\mathrm{p}' - k'\cos\theta)}{k'\sin\theta}. \tag{4.7}$$

Note that there is a threshold bandwidth of the pump envelope, which must be exceeded for the spectral uncorrelation of the state not to be destroyed by the strict spectral anti-correlation imposed by a narrow (or CW) pump,

$$\sigma_\mathrm{p} > \frac{\sqrt{2}}{\gamma L(k_\mathrm{p}' - k'\cos\theta)}, \tag{4.8}$$

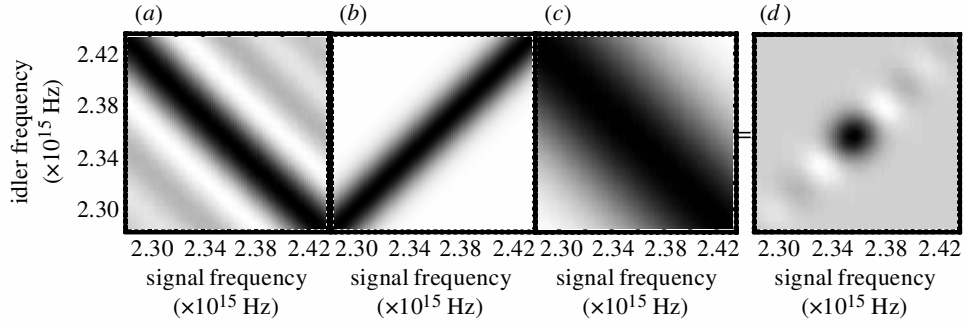

Figure 7. An uncorrelated two-photon state can be synthesized by exploiting transverse momentum in the crystal. Shown here is the case of a type-I BBO crystal pumped at 400 nm with output modes at $\pm 3^\circ$. (*a*) Longitudinal phase-matching function ($\phi_z(\Delta k_z)$); (*b*) transverse phase-matching function ($\phi^{\perp}(\Delta k^{\perp})$); (*c*) pump-envelope function with an FWHM bandwidth of 10 nm ($\alpha(\omega_s + \omega_i)$); (*d*) product of the three previous functions, or the joint spectral amplitude.

where σ_p refers to the pump bandwidth defined in § 2. Let us look at a specific example involving a 1000 µm long type-I BBO crystal with a cut angle of $\theta_{PM} = 30.32^\circ$. When pumping such a crystal with an ultrafast pulsed pump centred at $\lambda_p = 0.4$ µm, degenerate non-collinear PDC is phase matched at propagation angles (within the crystal) of $\theta_s = 3^\circ$ and $\theta_i = -3^\circ$. The condition in equation (4.7) gives a beam diameter of $w_0 = 287$ µm. Note that with $w_0/L = 0.287$ and $\theta = 3^\circ$ we are in a regime where the approximation $w_0/L \gg \sqrt{\gamma}\sin^2\theta$ is valid. Figure 7 shows graphically the interplay of the longitudinal and transverse phase-matching functions which combine to yield an uncorrelated state. Note that the down-converted photons are in this example emitted with a central wavelength of $\lambda = 0.8$ µm so that they can be conveniently detected with silicon-based detectors.

5. Summary

We have shown that it is crucial for the successful implementation of quantum information processing schemes in the photonic domain to specify the properties of the photons in all degrees of freedom, including those which are not of primary interest to the experiment in question. We have reported techniques for measuring the spatial properties and for engineering the spectral degree of freedom in photon pairs generated by the process of parametric down-conversion.

References

Banaszek, K. & Wódkiewicz, K. 1996 *Phys. Rev. Lett.* **76**, 4344–4347.

Bastiaans, M. J. 1978 *Opt. Commun.* **25**, 26–30.

Braunstein, S. L. & Mann, A. 1995 *Phys. Rev.* A **51**, R1727–R1730.

Brenner, K.-H. & Lohmann, A. W. 1982 *Opt. Commun.* **42**, 310–314.

Dorrer, C. & Walmsley, I. A. 2002 *Opt. Lett.* **27**, 1613–1615.

Grice, W. P. 1997 Interference and indistinguishability in ultrafast spontaneous parametric downconversion. PhD thesis, University of Rochester, NY.

Grice, W. P. & Walmsley, I. A. 1997 *Phys. Rev.* A **56**, 1627–1634.

Grice, W. P., U'Ren, A. B. & Walmsley, I. A. 2001 *Phys. Rev.* A **64**, 063815.

Hong, C. K., Ou, Z. Y. & Mandel, L. 1987 *Phys. Rev. Lett.* **59**, 2044–2046.

Iaconis, C. & Walmsley, I. A. 1996 *Opt. Lett.* **21**, 1783–1786.

Kim, Y. & Grice, W. P. 2002 *J. Mod. Opt.* **49**, 2309–2323.

Kim, Y., Kulik, S. P., Chekhova, M. V., Grice, W. P. & Shih, Y. 2003 *Phys. Rev.* A **67**, 010301.

Kwiat, P. G., Mattle, K., Weinfurter, H. & Zeilinger, A. 1995 *Phys. Rev. Lett.* **75**, 4337–4340.

Kwiat, P. G., Waks, E., White, A. G., Appelbaum, I. & Eberhard, P. H. 1999 *Phys. Rev.* A **60**, 773.

Lvovsky, I., Hansen, H., Aichele, T., Benson, O., Mlynek, J. & Schiller, S. 2001 *Phys. Rev. Lett.* **87**, 050402.

Nambu, Y., Usami, K., Tsuda, Y., Matsumoto, K. & Nakamura, K. 2002 *Phys. Rev.* A **66**, 033816.

Wax, A. & Thomas, J. E. 1996 *Opt. Lett.* **21**, 1427–1430.